Surface morphology of $Cr:Ga_2Se_3$ heteroepitaxy on Si(001)

E. N. Yitamben,[1,*] T. C. Lovejoy,[1] D. F. Paul,[2] J. B. Callaghan,[2] F. S. Ohuchi,[3] and M. A. Olmstead[1]
[1]*Department of Physics and Center for Nanotechnology (CNT), University of Washington, P.O. Box 351560, Seattle, Washington 98195, USA*
[2]*Physical Electronics, Chanhassen, Minnesota 55317, USA*
[3]*Department of Materials Science and Engineering and Center for Nanotechnology (CNT), University of Washington, P.O. Box 352120, Seattle, Washington 98195, USA*

(Received 18 February 2009; revised manuscript received 4 June 2009; published 21 August 2009)

Addition of the transition-metal dopant Cr to Ga_2Se_3 during heteroepitaxial growth on Si(001), a system of interest as a prototype silicon-compatible, dilute magnetic semiconductor, has been studied with scanning-tunneling microscopy and scanning Auger microscopy as a function of Cr concentration and the presence or absence of an undoped buffer or capping layer. Chromium incorporates into laminar Ga_2Se_3 films up to a solubility limit of several atomic percent, after which Cr-rich islands nucleate. At low Cr concentrations, the vacancy-ordered nanoridge structure characteristic of pure Ga_2Se_3 remains but nanoridge aspect ratios decrease with Cr concentration; this is likely associated with Cr removing intrinsic vacancies. At higher Cr concentrations, faceted, Cr-rich islands nucleate, often surrounded by trenches, and the terrace morphology no longer resembles pure Ga_2Se_3. Growth of Cr-doped Ga_2Se_3 directly on Si(001):As is qualitatively similar to growth on a pure Ga_2Se_3 buffer layer; however, the island structure changes dramatically upon coverage of a highly doped layer with undoped Ga_2Se_3. Addition of Cr stabilizes cubic overlayer growth under Se-poor growth conditions beyond that of pure Ga_2Se_3; no growth of the hexagonal layered structure characteristic of bulk GaSe was observed.

DOI: 10.1103/PhysRevB.80.075314 PACS number(s): 68.37.Ef, 68.35.Dv, 68.55.−a

I. INTRODUCTION

Transition-metal doping of semiconductors can dramatically alter the electronic, optical, and magnetic properties of both the dopant and host. For example, doping of GaN,[1] AlN,[2,3] ZnTe,[4] and TiO_2 (Refs. 5 and 6) with a few percent chromium leads to room-temperature ferromagnetism in these wide-bandgap semiconductors. Such dilute magnetic semiconductors (DMS) are of interest for spintronic applications;[7,8] however, with the possible exception of anatase TiO_2,[9–12] the difference in both lattice constant and ionicity precludes heteroepitaxial growth of these promising DMS materials on silicon.

Ga_2Se_3 is a defected-zinc-blende semiconductor (band gap ~2.5 eV) (Ref. 13) that may be grown epitaxially on silicon (lattice mismatch ~0.1%); its intrinsic vacancies lead to a highly anisotropic epitaxial film on Si(001) characterized by aligned, one-dimensional nanorods.[14] The combination of anisotropy, multiple dopant incorporation sites (Cr_{Ga} or Cr_V), and recent spin-dependent density-functional calculations predicting a ferromagnetic behavior for 5% Cr in Ga_2Se_3(at least at $T=0$ K),[15,16] leads us to investigate $Cr:Ga_2Se_3$ as a potential DMS.

Several bulk Ga-Cr-Se compounds with stoichiometry $(Ga_{1-x}Cr_x)_2Se_3$ have been reported, including $x=1/2$,[17,18] $x=2/5$,[19,20] and $x=1/3$ (referred to Refs. 18 and 19 and also reported as a sulfide[21]). These structures vary in symmetry but each exhibits intrinsic cation vacancies or voids and has Ga in a tetrahedral environment while Cr is in an octahedral environment. This raises the question of chromium's preferred location in the Ga_2Se_3 lattice at low concentrations (tetrahedral or octahedral) and whether new phases may nucleate. $GaCrSe_3$ is reported to be antiferromagnetic, with a Néel temperature of 88 K (Ref. 17) while $Ga_2Cr_{1.33}Se_5$ is reported to exhibit ferromagnetic magnetic interactions that are too weak to cause a magnetic transition.[19]

This paper takes the first step toward possible application of $Cr:Ga_2Se_3$ as a silicon-compabitible DMS, namely, investigation of the structure, morphology, and solubility limits of heteroepitaxial $Cr:Ga_2Se_3$ films on Si(001):As as a function of Cr concentration and the presence or absence of a pure Ga_2Se_3 layer above or below the Cr-doped film. Magnetic and x-ray absorption measurements will be reported elsewhere.[22] Scanning-tunneling microscopy (STM) reveals a surface locally similar to that of pure Ga_2Se_3 up to ~9 at. % Cr in the incident flux, although the nanorod aspect ratio decreases and occasional islands are observed. The size and number of islands increases with Cr concentration, indicating a solubility limit in the terraces. At higher concentrations, these 1–4-nm-tall islands are typically surrounded by ~1 nm-deep trenches and scanning Auger microscopy (SAM) shows the islands are Cr-rich compared to the flat regions between the islands. At the highest concentrations investigated (17% Cr), the island size and density decreases significantly upon addition of an undoped overlayer, although evidence of the trenches still remains as rectangular holes.

II. EXPERIMENT

Experiments were conducted in an ultrahigh-vacuum (UHV) system with base pressure $\lesssim 1\times10^{-10}$ torr. Si(001) samples were chemically cleaned to replace the commercial oxide, outgassed in UHV, flashed to ~1200 °C to remove the chemical oxide, and terminated with one monolayer of arsenic[23] by cooling from above 800 °C in an As_4 atmo-

 ©2009 The American Physical Society

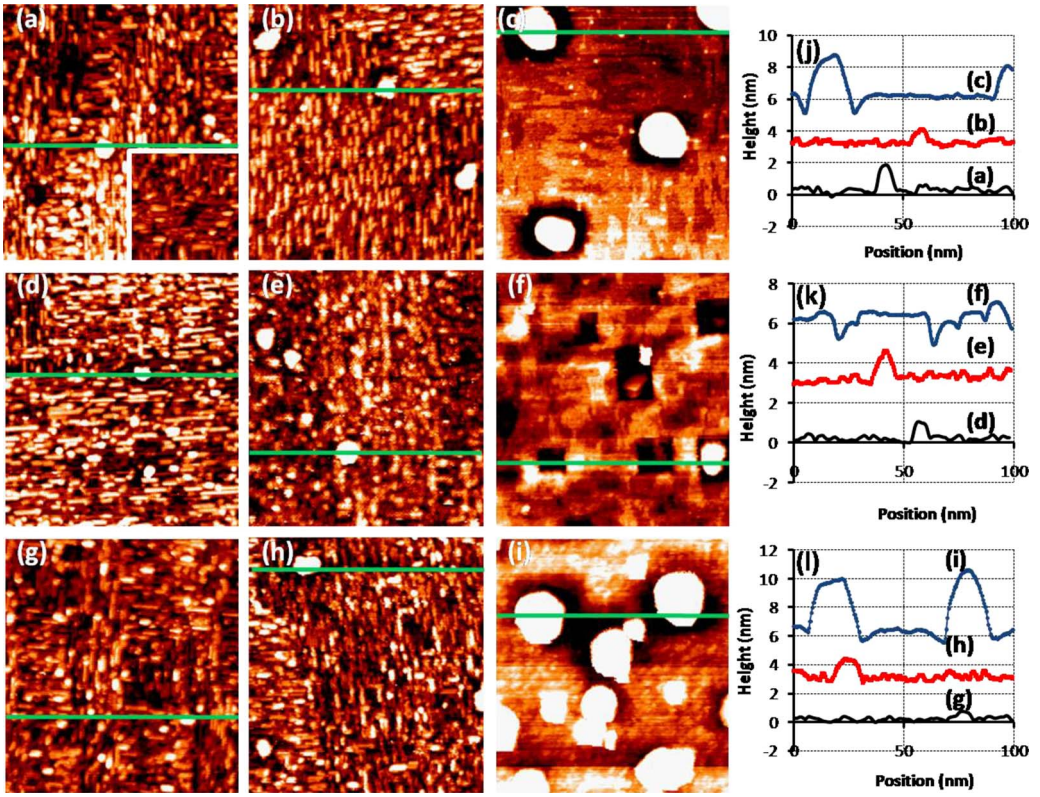

FIG. 1. (Color online) Surface topography of $Cr:Ga_2Se_3$ with STM (empty state images). Growth parameters of Cr concentration are: doped only for (a)–(c): (a) 6%, inset 3%; (b) 9%; (c) 17%; doped/pure for (d)–(f): (d) 6/0%; (e) 9/0%; (f) 16/0%; pure/doped for (g)–(i): (g) 0/6%; (h) 0/9%; (i) 0/17%. The right column shows line profiles along (green) lines from the above images: (j) doped only; (k) doped/pure; (l) pure/doped. STM images are 100×100 nm^2. Vertical scale color range = 0.6 nm except (i), where it is 1.2 nm. Additional information is in Table I.

sphere ($p_{As}\sim10^{-7}$ torr). Arsenic termination was used to prevent extensive reaction between the silicon and selenium.[24]

GaSe and Cr were simultaneously evaporated from distinct Knudsen cells. GaSe was evaporated at a rate of ~0.4–0.6 nm/min [measured via a quartz-crystal microbalance (QCM)] and Cr at a rate of ~0.02–0.04 nm/min at a nominal background pressure $p\sim10^{-9}$ torr and substrate temperature $T_{sub}\simeq475-500$ °C. Previous studies have shown the sticking coefficient for the first 2–3 bilayers of Ga_2Se_3 deposited on Si(001):As to be on the order of 1/3 (Ref. 25) although Cr may affect the sticking coefficient. Data presented here are from films showing a total GaSe +Cr accumulation on the QCM of 3–5 nm while x-ray photoemission spectroscopy (XPS) on nonislanded films indicates the resultant films (doped+undoped layers) were 1.5–3 nm thick. The incident flux has equal atomic percent Ga and Se but the resultant structure on Si(001) is cubic Ga_2Se_3 and not hexagonal GaSe. For flat, 3–4 nm films with 6% Cr in the incident flux, XPS showed a Ga:Se ratio 2/3 that of GaSe-bilayer terminated Si(111),[26] low-energy electron diffraction (LEED) showed a square pattern.

Below, films are labeled by the atomic percent Cr in the incident flux of (Cr+GaSe), although the actual Cr concentration in the film is likely to be different. Scaling from Hartree-Fock cross sections,[27] XPS measurements on a flat, 3-nm film with 6 at. % Cr in the incident flux had a Cr:(Cr+Ga) ratio of $x=0.08$.

Chromium atomic percents in the incident flux were nominally varied between 3% and 18%. Two different growth sequences were used: (1) codeposition of Cr and GaSe on the Si(001):As substrate, followed by an overlayer of pure Ga_2Se_3 and (2) deposition of a pure Ga_2Se_3 buffer layer, followed by codeposition of a doped layer. We use the notation A/B % to denote the nominal Cr concentrations in each layer, e.g., 6/0% for a film using growth sequence 1, with a 6 at. % Cr-doped film followed by an undoped layer, and 0/6% for the reverse, with growth sequence 2. The local Cr concentration is likely between A and B; e.g., for the 0/6% sample in Fig. 1(g), the undoped film had a QCM thickness of 1.3 nm and the doped film of 2.7 nm, for an average concentration of 4% if the Cr diffused freely.

The samples' surface structure was investigated using LEED and STM (Ref. 28) at each step: bare Si, arsenic terminated silicon, and after $Cr:Ga_2Se_3$ deposition. XPS measurements were obtained after STM to determine average elemental concentrations and chemical information. Subsequent *ex situ* measurements of local elemental information of island and terrace regions were obtained with a PHI 700 scanning Auger microscope and secondary electron microscope (SEM) on some samples.

III. RESULTS

The morphology of $Cr:Ga_2Se_3$ films on Si(001):As varies considerably with both Cr concentration and with the pres-

TABLE I. Parameters and description for Fig. 1. Cr concentration in atomic percent of atomic flux; thickness as integrated flux on the quartz crystal monitor, likely thicker than actual film. Island d, h are the average diameter and height, respectively, of islands in a 400 × 400 nm^2 area; f = fraction of that area covered by islands. V_s is the sample voltage relative to the tip.

Fig. 1 Image	Cr Conc A/B QCM thick	Overall Morphology	Islands	Trenches	Terraces	STM Params
a-inset	3% 3.9 nm	nanoridges very few islands	$d = 11$ nm $h = 0.9$ nm $f \lesssim 0.1\%$	no	resemble pure Ga_2Se_3	$V_s = 5.0$ V $I = 0.2$ nA
a	6% 2.9 nm	nanoridges plus occasional islands	$d = 10$ nm $h = 0.8$ nm $f = 0.3\%$	no	resemble pure Ga_2Se_3	$V_s = 5.0$ V $I = 0.2$ nA
b	9% 2.8 nm	nanoridges plus more, larger islands than *a*	$d = 12$ nm $h = 0.9$ nm $f = 2\%$	no	resemble pure Ga_2Se_3 though nanoridges are shorter and wider	$V_s = 3.34$ V $I = 0.2$ nA
c	17% 4.3 nm	Cr-rich, large, faceted islands surrounded by trenches in flat terrace	$d = 22$ nm $h = 2.6$ nm $f = 11\%$	yes	no nanoridges smooth, flat ML steps	$V_s = 5.0$ V $I = 0.2$ nA
d	6/0% 2.7/1.1 nm	nanoridges plus occasional islands similar to *a*	$d = 11$ nm $h = 0.8$ nm $f = 0.2\%$	no	resemble pure Ga_2Se_3	$V_s = 5.0$ V $I = 0.2$ nA
e	9/0% 2.8/1.3 nm	nanoridges plus medium sized islands similar to *b*	$d = 11$ nm $h = 0.8$ nm $f = 0.8\%$	no	resemble pure Ga_2Se_3 though nanoridges are shorter and wider	$V_s = 5.0$ V $I = 0.2$ nA
f	16/0% 2.7/2.3 nm	dramatic reduction of island height from *c*, plus rectangular holes, 1 − 5 nm deep, 20 nm wide	$d = 15$ nm $h = 1.1$ nm $f = 5\%$	yes	no nanoridges smooth, flat with 1 − 5 nm deep holes	$V_s = 5.0$ V $I = 0.2$ nA
g	0/6% 1.2/2.7 nm	nanoridges plus occasional islands similar to *a*	$d = 9$ nm $h = 0.5$ nm $f = 0.3\%$	no	resemble pure Ga_2Se_3	$V_s = 5.0$ V $I = 0.2$ nA
h	0/9% 1.1/2.7 nm	nanoridges plus medium sized islands similar to *b*	$d = 11$ nm $h = 0.8$ nm $f = 0.6\%$	no	resemble pure Ga_2Se_3 though nanoridges are shorter and wider	$V_s = 3.34$ V $I = 0.2$ nA
i	0/17% 2.3/2.7 nm	Cr-rich, large, faceted islands with trenches, higher density than *c*	$d = 20$ nm $h = 2.4$ nm $f = 16\%$	yes: large islands no: small islands	no nanoridges rougher than *c* or *f*, ML steps	$V_s = 5.0$ V $I = 0.2$ nA

ence or absence of an undoped layer. Figure 1 shows STM images of 100×100 nm^2 regions for different Cr concentrations with and without an undoped buffer layer or overlayer. Films with the same nominal Cr concentration in the doped layer are in vertical columns—6% [Figs. 1(a), 1(d), and 1(g)], 9% [Figs. 1(d), 1(e), and 1(h)] and 17% [Figs. 1(c), 1(f), and 1(i)]—while the rows show the same growth sequence: doped only [Figs. 1(a)–1(c)], doped/pure [Figs. 1(d)–1(f)] and pure/doped [Figs. 1(g)–1(i)]. The last column [Figs. 1(j)–1(l)] shows height as a function of lateral position along the lines marked in Figs. 1(a)–1(i). The inset in Fig. 1(a) is from a 3% Cr film (50×50 nm^2). Details of the growth and measurements are given in Table I.

In all cases, LEED shows a square 1×1 pattern with lattice constant indistinguishable from the underlying silicon. Streaks connect the diffraction spots, similar to the pattern observed for undoped Ga_2Se_3/Si(001):As; however, in the doped case, the streaks are broader and less intense relative to the sharp 1×1 spots.

STM images of Cr-doped films deposited directly on As-terminated Si(001) are shown in the top row of Fig. 1 with an expanded view of nonislanded regions in Fig. 2. At low concentrations [Figs. 1(a) and 2(c)], the film shows a nanoridge structure similar to undoped Ga_2Se_3 [Fig. 2(b)],[14] except that the [110]-oriented nanoridges are shorter and slightly wider than in the undoped case, and there are occasional small islands (typical diameter ~10 nm, height $\lesssim 1-2$ nm, concentration about 5 in a 200×200 nm^2 region for 6% film, <1 in the same area for 3% film). At somewhat higher Cr concentrations [9%, Fig. 1(b)], the islands have a higher density and larger diameter, but are still $\lesssim 1-2$ nm high and the area between the islands again resembles pure Ga_2Se_3 but with still wider structures [Fig. 2(d)].

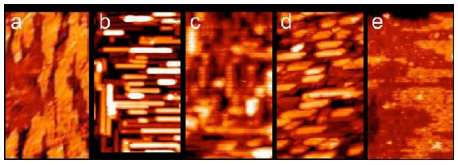

FIG. 2. (Color online) Expanded STM view of regions between islands for (a) pure Ga_2Se_3 (1.5 bilayers) [−4 V, 0.09 nA]; (b) pure Ga_2Se_3 (3.2 bilayers) [−5.4 V, 0.09 nA]; (c) 3% film in Fig. 1(a) inset; (d) 9% film in Fig. 1(b); and (e) 17% film in Fig. 1(c). (25×42 nm^2, color z scale range 0.6 nm), images (a) and (b) adapted from Ref. 25.

At still higher Cr concentrations [17%, Figs. 1(c) and 2(e)] the structure qualitatively changes. The area between the islands no longer exhibits well-defined nanoridges, although some directionality in the one-bilayer-deep holes may be seen, similar to 0.5-nm thick Ga_2Se_3[Fig. 2(a)].[25] Large islands are observed with a typical diameter ~18–25 nm and height ~4–5 nm with some smaller islands also observed. The larger islands are surrounded by ~1 nm-deep trenches; trench edges show general alignment with the substrate [110] and [1$\bar{1}$0] directions.

Capping the islanded Cr-doped films with additional undoped Ga_2Se_3, as shown in the middle row of Fig. 1, makes small changes in the morphology at low concentrations [Figs. 1(d) and 1(e)], but dramatically changes the sample morphology at high concentrations [Fig. 1(f)]. For low doping [Fig. 1(d)], adding 1.3 nm of pure Ga_2Se_3 to the 6% film in Fig. 1(a) results in fewer, smaller islands than the uncovered film, with larger area scans showing only ~1 island taller than 2 bilayers high per 200×200 nm^2 region. At intermediate doping [Fig. 1(e)], addition of 1.3-nm undoped Ga_2Se_3 to the 2.7-nm 9% Cr film in Fig. 1(b) does not significantly change the island morphology, although the nanoridge structure between the islands is less well defined. In contrast, adding 2.3 nm to a 2.8 nm high Cr concentration film (16%) [Fig. 1(f)], leads to a dramatic reduction in the island size with capping, plus creation of ~1.5 nm-deep, ~20 nm-wide rectangular holes scattered over the surface. Many of these holes have islands in them that occasionally rise above the average level of the surface.

Deposition of Cr-doped Ga_2Se_3 on top of an undoped Ga_2Se_3 buffer layer is shown in the bottom row of Fig. 1. At low Cr concentration [0/6%, Fig. 1(g)], the [110]-nanoridge structure is again evident, and very few islands taller than 2 bilayers (0.5 nm) are observed [none in Fig. 1(g)]. At higher concentrations [0/9%, Fig. 1(h)], small islands are observed similar to the 9/0% and 9% films. Other 0/9% films grown more slowly (0.4 nm/min instead of 0.6 nm/min) and with thinner buffer layers show taller islands surrounded by trenches similar to the 17% film in Fig. 1(c); an example is in Fig. 3(b). At still higher concentrations [0/17%, Fig. 1(i)], both the size and density of the islands is increased over both the 0/9% and 17% films (largest island diameters ~30 nm, and height ~3–5 nm, although many smaller islands are also observed) and ~15% of the surface is covered by islands. The region between the islands on the 0/17% film is much rougher than for the lower concentration films [note color range z scale is doubled in Fig. 1(i); it is constant for the remaining images in Fig. 1]. Most of the large islands are surrounded by nm-deep trenches, though several smaller islands are not. The STM tip likely does not reach the bottom of the trenches due to interactions with the island and trench edges.

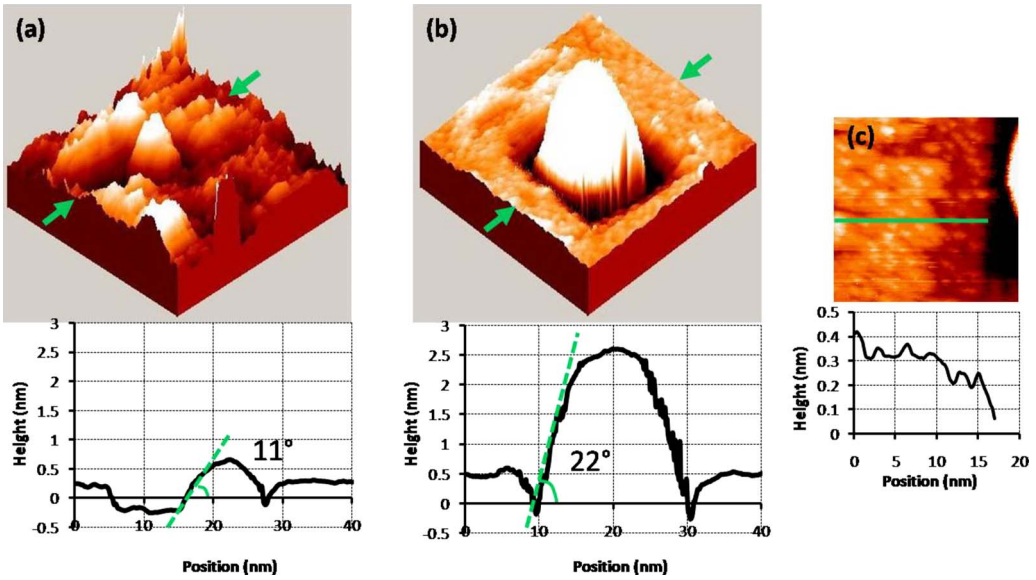

FIG. 3. (Color online) Local structure of Cr:Ga_2Se_3 island regions with STM. (a) Three-dimensional (3D) profile expanded region of 16% (2.7 nm)+0% (2.3 nm) sample shown in Fig. 1(f) (5V tip, 0.2 nA, and 42×42 nm^2). Island top 0.4 nm above the surrounding surface while sitting in a 0.4-nm-deep depression; (b) 3D profile of expanded region of 0% (1.3 nm) +9% (4.7 nm) sample (3.34 V tip, 0.2 nA, and 42×42 nm^2). Island top is 2-nm higher than the surrounding surface, in a 0.8-nm-deep depression; (c) expansion of flat area to the lower left of the island for 0/9% film in (b); and the white spots are about 2-nm apart (3.34V, 0.2nA, and 20×20 nm^2). The bottom row shows line profiles from the above images and the arrows indicate the line along which the 3D profile was taken while the dotted lines on the profiles show the facet angle.

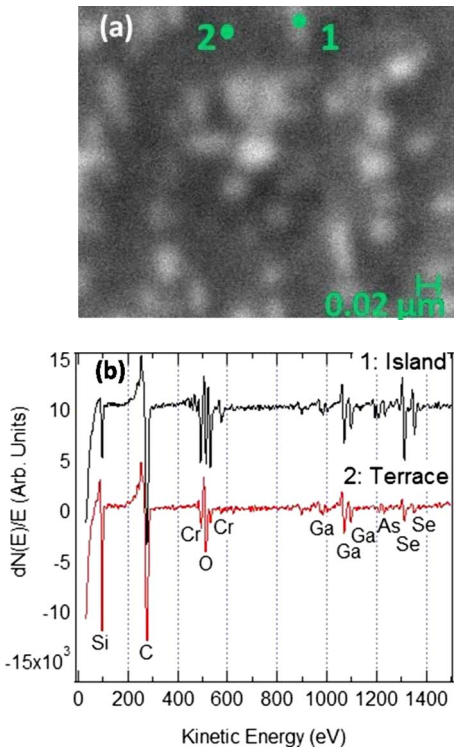

FIG. 4. (Color online) (a) SEM image of the surface of 16/0% sample in Figs. 1(f) and 3(a) (Field of view: 0.3 μm; 20.0 keV; and scale bar is 0.02 μm) and (b) spot Auger profiles from points marked in (a), revealing differential local composition between terrace and island regions. Approximate electron-beam size ~10 nm.

An expanded view of islands and trenches is shown in Fig. 3. Similar to most large islands in doped films, whether deposited either directly on the substrate or on an undoped buffer layer, the sides of the island in Fig. 3(b) are consistently about 22° from horizontal and the top has large regions parallel to the surface. The island sides are in general oriented parallel to the trench edges, along $[1\bar{1}0]$ and [110]. If the islands are cubic, their sides could be (205) facets. Smaller islands on films with either growth sequence [such as that in Fig. 3(a)] have facet angles of $8° \pm 1°$ and $11° \pm 1°$ [(105) and (107), if cubic]; those on uncapped films are less likely to sit within trenches. The smallest islands are only about 2 BL high, so that a facet angle is neither well defined nor independent of tip geometry.

The local terrace structures shown in Fig. 3 differ with growth sequence. While neither film shows a clear nanoridge structure, the 0/9% film shows ~0.05 nm tall protrusions spaced about 2 nm apart in occupied state images [bright, white spots in Fig. 3(c)]. They are not observed for films where the Cr-doped layer is buried beneath pure Ga_2Se_3. These features are similar to those observed for Co:TiO_2 (Ref. 9) and are likely due to Cr-induced states near the film surface. The step heights in Fig. 3(c) are 0.13 nm, reflecting single-height steps in the underlying Si lattice.

The local elemental composition and large-scale morphology of the 16/0% sample shown in Figs. 1(f) and 3(a) was measured with *ex situ* scanning Auger microscopy and SEM. The SEM image in Fig. 4(a) reveals a compositional difference between the darker uniform regions and the bright spots that have a density comparable to the density of larger islands observed with STM. We thus associate the darker regions with the area between islands and the bright spots with islands.

Auger spectra from a terrace region (point 2) and an island (point 1) taken with a ~10 nm diameter electron beam are shown in Fig. 4(b). The islands have more Auger electron spectroscopy emission from Cr, Se, and Ga and less from Si than do the terraces. This confirms that the bright spots are Cr-Ga-Se islands with thickness on the order of one escape depth more than that of the surrounding terrace. The Cr:Ga ratio is 1.7 times higher in spectrum 1 (island) than in spectrum 2 while the (Cr+Ga):Se ratio is 2.1 times higher in spectrum 2 (terrace) than in 1 [Fig. 4(b)]. The oxygen and carbon signals show minimal spatial dependence and likely arise from atmospheric exposure of the sample in transit from the STM to SAM. *In situ* XPS measurements immediately following STM measurements showed negligible oxygen and carbon but strong oxygen emission was observed after exposure of the sample to ambient atmosphere. Comparison of XPS spectra before and after atmospheric exposure showed a reduction in the Se:As ratio by nearly a factor of 2 and conversion of about 15% of the Cr signal to a higher binding-energy component (likely oxidized Cr).

IV. DISCUSSION

These results show that several atomic percent of Cr may be incorporated into Ga_2Se_3 without drastic changes in the crystal structure or morphology. As the Cr concentration increases further, islands begin to nucleate. The fractional volume in the islands rises with Cr concentration, with increases in island height, area, and number density. Large faceted islands are typically surrounded by a depression in the surrounding terrace. These islands change dramatically with addition of pure Ga_2Se_3 but are still Cr rich relative to the terrace regions. The terrace-region structure changes slowly with increasing Cr concentration until large islands nucleate, at which point the nanoridge structure disappears. These results are discussed below.

At low Cr concentrations, Cr-doped Ga_2Se_3 growth on Si(001):As looks similar to pure Ga_2Se_3, although the average width of the vacancy-induced nanoridges increases with Cr concentration while the average length decreases. Increased width is consistent with Cr eliminating vacancies, thus increasing the spacing between vacancy rows on the surface. Both increased width and decreased length could be induced by Cr-termination of a nanoridge reducing the adatom-attachment probability. A distinct difference between growth of lightly doped and pure films is the persistence of cubic growth for Cr:Ga_2Se_3 to at least ten times the 2-nm thickness at which pure Ga_2Se_3 converts to layered GaSe (the source material) under the same growth conditions.[25] Cr stabilization of the underlying zinc-blende structure at a higher cation:anion ratio (Cr eliminating vacancies) and/or inhibited incorporation of Cr into the cation-cation bonds of layered GaSe may lead to this difference.

At the lowest Cr concentration investigated, 3%, large ($>500 \times 500$ nm^2) island-free regions are observed; this is

also true for 0/6% films, though not for 6% or 6/0% films. A similar reduction in island density with a buffer layer is also observed for the 9% films, with a lower island density for the 0/9% film than for the 9% film deposited directly on Si(001):As. Surface-sensitive photoemission spectroscopy on similarly prepared films shows significant vertical diffusion of Cr that would reduce the surface Cr concentration in $0/X\%$ films[22] and diffusion should exhibit low-activation barriers in this intrinsic vacancy material. Thus, reduced islanding in $0/X\%$ films may be attributed to a lower effective Cr concentration during deposition as Cr interdiffuses. A reduced lateral diffusion barrier on Si(001):As relative to Ga_2Se_3 could also promote island formation and growth in films without a buffer layer.

The observed increase in island size and density with Cr concentration is consistent with precipitation of a $(Ga_{1-x}Cr_x)_2Se_3$ compound above a solubility limit. A simple substitution of Cr for Ga is not unreasonable at low concentrations since both Cr and Ga commonly take a 3^+ valence state and the atomic radii of Cr^{3+} and Ga^{3+} are within 1%. However, stoichiometric bulk $(Ga_{1-x}Cr_x)_2Se_3$ compounds $(x=1/3,2/5,1/2)$ have octahedrally coordinated Cr, with Cr-Se bond lengths 7–9 % longer than the tetrahedral Ga-Se bonds in either the same compound or pure Ga_2Se_3.[18,19] Thus, above a critical concentration, Cr is likely to alter the structure to accommodate a local octahedral environment. The difference in facet angles between the smaller islands that dominate at intermediate concentrations and the larger islands at high concentrations may indicate distinct phases for the two island types. We also note that photoemission shows the flat films to be semiconducting, while the islanded films are metallic.

The SAM results in Fig. 4 indicate the islands are chromium rich relative to their surroundings. While the dramatic change in morphology with capping for the 16/0% film measured with SAM implies extensive intermixing between the doped and undoped materials, the material closest to the surface of both the terrace and island regions is still likely Cr-poor relative to material closer to the interface. The increased relative intensity of the interface contribution to the Auger signal for the thinner terrace region implies the relative enrichment of Cr in the islands is larger than the value of 1.7 obtained from Fig. 4 and could be significantly larger in uncapped islands.

The *ex situ* SAM result of a reduced Se:cation ratio in terrace regions relative to islands may be attributed to a combination of surface oxidation and interface arsenic. Exposure to water vapor leads to loss of surface Se. Studies on pure Ga_2Se_3 show the As monolayer diffuses into Se sites for the first few bilayers so the Se:Ga ratio increases with thickness.[14,25] Since the surface plus interface is a much larger fraction of the thinner terrace regions than of the islands, the terraces will appear Se-poor relative to the islands.

The As Auger spectral region overlaps with a weaker Se transition, and the increase in signal around 1200–1250 eV between the terrace and island is primarily due to Se as opposed to the single monolayer of As. While it is possible that the islands have a different As content than the terrace regions, and that this may help stabilize the increased Cr concentration, there is insufficient As for the islands to be GaAs aggregates.

In films with small islands (<2 nm high, <10 nm diameter, and $<5\%$ surface coverage), islands are most often found near step edges where the nanoridge orientation switches by 90° and are typically bordered by a 1–2 bilayer deep ring on the lower terrace. Steps or kinks are locations where locally high Cr concentrations may be generated so that Cr-rich islands could nucleate there before the average Cr concentration is above the solubility limit. The 6% film in Fig. 1(a), where $<1\%$ of the film volume in islands, gives a rough lower limit on the Cr solubility.

Films with large islands (2–5 nm high, and 10–20 nm diameter) have terraces that do not exhibit a distinct nanorod structure [Figs. 1(c), 1(f), 1(i), 2(e), and 3], although they still show a 1×1 LEED pattern and step edges parallel to [110] and $[1\bar{1}0]$. Rather, the structure resembles $\lesssim0.5$ nm-thick pure Ga_2Se_3 on Si(001):As [Fig. 2(a)], where it is attributed to As incorporation reducing the vacancy concentration (Se-terminated GaAs has no vacancies).[25,29] The trenches surrounding Cr-Ga-Se islands, however, are deeper than the 3 bilayers at which the $Ga_2Se_3/Si(001):As$ structure stabilizes in narrow nanoridges, implying either that the trenches involve major silicon diffusion while the terrace regions are only 1–2 bilayers thick or that Cr-saturated Ga_2Se_3 results in a similar structure to Ga-As-Se. Since the step structure in the terraces reflects the single-atom-high step height of the Si substrate, major motion of Si is unlikely; XPS also indicates the terraces are thicker than 1–2 bilayers. Rather, the results are consistent with Cr occupation of vacancies reducing the need for vacancy rows, similar to As substitution for Se in the ultrathin Ga_2Se_3.

At intermediate Cr concentrations, small changes in growth conditions can impact the island nucleation. For example, the films depicted in Fig. 1(h) (small islands + nanoridge terraces) and in Fig. 3(b) (large islands + no nanoridges) are both 0/9% growths but the latter had a thinner pure layer (1.0 vs 1.3 nm on QCM) and a lower GaSe flux (0.4 vs 0.6 nm/min). The doped layer for Fig. 3(b) is also thicker than for Fig. 1(h) (4.2 vs 2.7 nm) but similar morphology to Fig. 3(b) was also seen for a 0/9% film with a 3.0-nm doped layer with the lower flux rate and thinner buffer layer. At a lower flux rate, it is more likely that Cr will diffuse to a high-concentration island before incorporating into the terrace, enhancing island growth, and thinner buffer layer will result in a higher effective Cr concentration during the nucleation stage. More important, however, is that these nominally 1.0-nm Ga_2Se_3 layers (actual thickness $\lesssim0.4$ nm) were too thin to develop the nanoridge structure of Fig. 2(b) but rather were similar to Fig. 2(a). This could lead both to epitaxial growth of a Cr-doped phase without ordered vacancies in the terraces and easier nucleation of Cr-rich islands arising from decreased diffusion barriers on this disordered surface.

When the surface layer is Cr doped, the terrace region shows bright 0.05-nm protrusions in empty state images likely associated with Cr electronic states. Similar features were attributed to Co states in Co-doped TiO_2 films,[9,35] and theoretical calculations for $CrGa_8Se_{12}$ (Cr on vacancy) show unoccupied Cr states 2–3 eV above the Fermi level.[15,16] It was not possible to obtain stable imaging under negative bias

(occupied states). The terrace region on the islanded 0/9% film in Figs. 3(b) and 3(c) shows about 25–30 protrusions per 100 nm^2 (2-nm average spacing), or about 4% of the surface sites; most of the bright spots are larger than the occasional small protrusions, however, which may imply multiple Cr atoms in most of the bright spots. This is consistent with the solubility estimate given above of about twice this value. The bright spots are randomly distributed as opposed to in [110] lines, so that while Cr may be replacing vacancies, the Cr-Ga distribution appears to be randomized. From the SAM measurements, the islands have at least twice the terrace Cr concentration. The large islands show edge alignment parallel to [110] and $[1\bar{1}0]$, which is more consistent with the monoclinic $x=1/3$ or orthorhombic $x=1/2$ $(Ga_{1-x}Cr_x)_2Se_3$ compounds than with the hexagonal ($x=0.4$) compound.

At higher concentrations and/or thicker films, large islands are surrounded by rectangular trenches up to 1.5-nm deep. They may reach the full terrace film thickness, though for small islands they are only 1–2 bilayers deep [see dark rings around islands in Figs. 1(b), 1(d), and 1(h)]. Similar trench-island morphologies are often seen for highly strained heteroepitaxy where intermixing reduces strain, such as Ge on Si (Ref. 30) and InAs on GaAs,[31,32] and for intermetallic growth such as CuInGaSe,[33] where rapid Cu diffusion driven by a chemical-potential gradient can lead to formation of Kirkendall voids.[34,36,37] While either mechanism may be relevant, the latter is more likely if the islands are precipitates of a stoichiometric phase. Creation of trenches for Ge/Si or InAs/GaAs involves substrate atom diffusion to dilute the overlayer phase and hence reduce its lattice constant; this mechanism for trench creation would require stability of a Cr-Ga-Se alloy over a wide range of concentrations with the same lattice structure as the substrate. On the other hand, if the islands are a new stoichiometric phase with a higher Cr concentration than the incident flux, there will be a chemical-potential gradient driving Cr into the islands and vacancies into the surrounding region. The trenches have more volume than simply the coalesced vacancies might predict, however and thus may have a strain-induced component, as well.

When pure Ga_2Se_3 is added to low-concentration Cr:Ga_2Se_3 films with small islands, there are no major changes in diameter, height, or density. However, when pure Ga_2Se_3 is added to strongly islanded films (islands >2 nm high, terraces without nanoridges), the islands shrink and/or disappear. A possible explanation is reversal of the Cr chemical-potential gradient, inducing out-diffusion of Cr from the islands into the undoped cap layer, leading the islands to revert to a zinc-blende-based structure once there is insufficient Cr to retain the crystal structure of the stoichiometric compound. The remaining holes on the surface may reflect a lower energy for further Ga_2Se_3 growth on the base layer than on uncovered substrate at the base of the hole.

V. CONCLUSION

In summary, up to several atomic percent Cr may be incorporated into the basic defected-zinc-blende structure of epitaxial Ga_2Se_3 on Si(001):As. The aspect ratio of the nanorod structure associated with vacancy ordering decreases with increasing Cr concentration. This may be explained by Cr occupying vacant sites, though additional substitution of Cr for Ga cannot be ruled out; the Cr appears randomly distributed among cation sites. Above a solubility limit of 6–9 % in the incident flux, Cr-rich islands nucleate. The largest islands are faceted and likely reflect precipitation of stoichiometric compound with rectangular in-plane symmetry while the smaller islands may be a Cr-rich zinc-blende phase. Large islands are surrounded by trenches and are restructured upon capping with pure Ga_2Se_3; we propose these morphologies result from diffusion driven by a Cr chemical-potential gradient between terraces and Cr-rich islands. The ability to grow laminar films of cubic Cr:Ga_2Se_3 to several atomic percent Cr bodes well for investigation of this material as a silicon-compatible dilute magnetic semiconductor.

ACKNOWLEDGMENTS

This work is supported by the NSF under Grant No. DMR 0605601. E.N.Y. further acknowledges support from the IBM Corporation, and T.C.L. from the IGERT through the University of Washington. The data for Figs. 2(a) and 2(b) is taken from T. Ohta (University of Washington, 2004).

*yitamben@u.washington.edu

[1] M. B. Haider, R. Yang, H. Al-Brithen, C. Constantin, D. C. Ingram, A. R. Smith, G. Caruntu, and C. O'Connor, J. Cryst. Growth **285**, 300 (2005).
[2] R. K. Singh, Stephen Y. Wu, H. X. Liu, Lin Gu, David J. Smith, and N. Newman, Appl. Phys. Lett. **86**, 012504 (2005).
[3] H. X. Liu, Stephen Y. Wu, R. K. Singh, Lin Gu, David J. Smith, N. Newman, N. R. Dilley, L. Montes, and M. B. Simmonds, Appl. Phys. Lett. **85**, 4076 (2004).
[4] H. Saito, V. Zayets, S. Yamagata, and K. Ando, Phys. Rev. Lett. **90**, 207202 (2003).
[5] T. C. Kaspar, S. M. Heald, C. M. Wang, J. D. Bryan, T. Droubay, V. Shutthanandan, S. Thevuthasan, D. E. McCready, A. J. Kellock, D. R. Gamelin, and S. A. Chambers, Phys. Rev. Lett. **95**, 217203 (2005).
[6] T. C. Kaspar, T. Droubay, V. Shutthanandan, S. M. Heald, C. M. Wang, D. E. McCready, S. Thevuthasan, J. D. Bryan, D. R. Gamelin, A. J. Kellock, M. F. Toney, X. Hong, C. H. Ahn, and S. A. Chambers, Phys. Rev. B **73**, 155327 (2006).
[7] S. A. Wolf, D. D. Awschalom, R. A. Buhrman, J. M. Daughton, S. von Molnár, M. L. Roukes, A. Y. Chtchelkanova, and D. M. Treger, Science **294**, 1488 (2001).
[8] T. Dietl, J. Appl. Phys. **89**, 7437 (2001).
[9] D. A. Schmidt, Taisuke Ohta, C.-Y. Lu, A. Bostwick, Q. Yu, Eli Rotenberg, F. S. Ohuchi, and M. A. Olmstead, Appl. Phys. Lett. **88**, 181903 (2006).
[10] R. A. McKee, F. J. Walker, and M. F. Chisholm, Phys. Rev. Lett. **81**, 3014 (1998).

[11] R. A. McKee, F. J. Walker, M. B. Nardelli, W. A. Shelton, and G. M. Stocks, Science **300**, 1726 (2003).
[12] C. C. Fulton, G. Lucovsky, and R. J. Nemanich, Appl. Phys. Lett. **84**, 580 (2004).
[13] M. Peressi and A. Baldereschi, J. Appl. Phys. **83**, 3092 (1998).
[14] Taisuke Ohta, D. A. Schmidt, Shuang Meng, A. Klust, A. Bostwick, Q. Yu, M. A. Olmstead, F. S. Ohuchi, Phys. Rev. Lett. **94**, 116102 (2005).
[15] Ngigi wa Gatuna, Ph.D. dissertation, University of Washington, 2007.
[16] E. N. Yitamben, I. N. Gatuna, T. C. Lovejoy, F. S. Ohuchi, and M. A. Olmstead (unpublished).
[17] A. A. Zhukov, Ya. A. Kesler, V. F. Meshcheryakov, and A. V. Rozantsev, Sov. Phys. Solid State **25**, 1328 (1983).
[18] H. D. Lutz, B. Engelen, M. Fischer, and M. Jung, Z. Anorg. Allg. Chem. **566**, 55 (1988).
[19] I. Okonska-Kozłowska, K. Szamocka, E. Malicka, A. Waskowska, J. Heimann, T. Mydlarz, A. Gilewski, and T. Gron, J. Alloys Compd. **366**, 21 (2004).
[20] D. Skrzypek, I. Okonska-Kozłowska, K. Szamocka, and E. Malicka, J. Magn. Magn. Mater. **285**, 379 (2005).
[21] H. Haeuseler, W. Kwarteng-Acheampong, and M. Jung, J. Phys. Chem. Solids **49**, 767 (1988).
[22] E. N. Yitamben, T. C. Lovejoy, A. Pakhemov, F. S. Ohuchi, and M. A. Olmstead (unpublished).
[23] R. D. Bringans, D. K. Biegelsen, and L.-E. Swartz, Phys. Rev. B **44**, 3054 (1991).
[24] R. D. Bringans, D. K. Biegelsen, L.-E. Swartz, F. A. Ponce, and J. C. Tramontana, Phys. Rev. B **45**, 13400 (1992).
[25] T. Ohta, Ph.D. dissertation, University of Washington, 2004.
[26] S. Meng, B. R. Schroeder, and M. A. Olmstead, Phys. Rev. B **61**, 7215 (2000).
[27] J. J. Yeh and I. Lindau, At. Data Nucl. Data Tables **32**, 1 (1985).
[28] Omicron Nanotechnology GmBH, Germany.
[29] C.-Y. Lu, Ph. D. dissertation, University of Washington, 2007; C.-Y. Lu, T. Ohta, F. S. Ohuchi, and M. A. Olmstead (unpublished).
[30] G. Katsaros, A. Rastelli, M. Stoffel, G. Isella, H. von Kanel, A. M. Bittner, J. Tersoff, U. Denker, O. G. Schmidt, G. Costantini, and K. Kern, Surf. Sci. **600**, 2608 (2006).
[31] Zh. M. Wang, J. H. Lee, B. L. Liang, W. T. Black, Vas. P. Kunets, Yu. I. Mazur, and G. J. Salamo, Appl. Phys. Lett. **88**, 233102 (2006).
[32] N. Nuntawong, J. Tatebayashi, P. S. Wong, and D. L. Huffaker, Appl. Phys. Lett. **90**, 163121 (2007).
[33] C. Lei, A. Rockett, I. M. Robertson, W. N. Shafarman, and M. Beck, J. Appl. Phys. **100**, 073518 (2006).
[34] A. D. Smigelskas and E. O. Kirkendall, Trans. Am. Inst. Min., Metall. Pet. Eng. **171**, 130 (1947).
[35] J. S. Yang, D. H. Kim, S. D. Bu, T. W. Noh, S. H. Phark, Z. G. Khim, I. W. Lyo, and S.-J. Oh, Appl. Phys. Lett. **82**, 3080 (2003).
[36] C. H. Lei, A. A. Rockett, I. M. Robertson, N. Papathanasiou, and S. Siebentritt, J. Appl. Phys. **100**, 114915 (2006).
[37] Yadong Yin, Robert M. Rioux, Can K. Erdonmez, Steven Hughes, Gabor A. Somorjai, and A. Paul Alivisatos, Science **304**, 711 (2004).